Hindawi
Geofluids
Volume 2018, Article ID 9410890, 12 pages
https://doi.org/10.1155/2018/9410890

Research Article

Consolidated and Undrained Ring Shear Tests on the Sliding Surface of the Hsien-du-shan Landslide in Taiwan

Hung-Ming Lin,[1] Jian-Hong Wu,[2] and Erik Sunarya[2]

[1]*Sustainable Environment Research Laboratories, National Cheng Kung University, Tainan, Taiwan*
[2]*Department of Civil Engineering, National Cheng Kung University, Tainan 701, Taiwan*

Correspondence should be addressed to Jian-Hong Wu; jhwu@mail.ncku.edu.tw

Received 18 April 2018; Revised 14 August 2018; Accepted 18 September 2018; Published 30 October 2018

Guest Editor: Xueyu Pang

A new consolidated undrained ring shear test capable of measuring the pore pressures is presented to investigate the initiation mechanism of the Hsien-du-shan rock avalanche, triggered by Typhoon Morakot, in southern Taiwan. The postpeak state of the landslide surface between the Tangenshan sandstone and the remolded landslide gouge is discussed to address the unstable geomorphological precursors observed before the landslide occurred. Experimental results show that the internal friction angle of the high water content sliding surface in the total stress state, between 25.3 and 26.1°, clarifies the reason of the stable slope prior to Typhoon Morakot. In addition, during the ring shear tests, it is observed that the excess pore pressure is generated by the shear contractions of the sliding surface. The remolded landslide gouge, sheared under the high normal stress, rendered results associated with high shear strength, small shear contraction, low hydraulic conductivity, and continuous excess pore pressure. The excess pore pressure feedback at the sliding surface may have accelerated the landslide.

1. Introduction

In 2009, the Hsien-du-shan landslide, triggered by Typhoon Morakot [1, 2], killed more than 400 people at the Hsiaolin village, Kaohsiung, Taiwan. Before this landslide mobilized, the authority announced two potential debris flow torrents (Kaohsiung County DF06 and DF07) (http://246.swcb.gov.tw/allfiles/PDF/98%E5%B9%B4%E8%8E%AB%E6%8B%89%E5%85%8B%E9%A2%B1%E9%A2%A8-%E9%AB%98%E9%9B%84%E7%94%B2%E4%BB%99-001-(%E9%80%9F).pdf) as major threats to the local residents in the Hsiaolin village. The debris flow damaged the village during the Kalmaegi in 2008. However, the historical record was unavailable to warn the residents that the village is located at a geological site with a large unstable slope.

The Hsien-du-shan landslide had demanded the authorities to respond urgently in developing new technologies for warning the occurrence of a rainfall-induced rock avalanche. In addition to detecting an abnormal geomorphological pattern [3, 4], clarification of the initiation mechanism of a large rock avalanche is another important task to mitigate disasters (Chen and Wu (2018); Hung et al. (2018); [5]). Figure 1 shows the available mathematical models to describe the mechanical behavior of the sliding surface of the Hsien-du-shan landslide. A conventional constant friction coefficient was applied to different numerical methods to simulate the postfailure behavior (dashed line) (Figure 1) [1, 2, 6]. Kuo et al. [7] discovered experimentally slip weakening by the colluvium on the sliding surface that was within the range of natural water contents using high-speed rotary shear tests with maximum shear speed and shear displacement of up to 1.3 m/s and 90 m, respectively (solid lines). Slip weakening is defined as a significant decrease in the friction angle of a sliding surface under high-speed sliding. However, the friction models in Figure 1 did not explicitly consider the pore pressure changes during the Hsien-du-shan landslide. But, studies [8–10] highlighted the importance of including changes in pore pressure to clarify the triggering process of a sliding surface. Lee and Delaney [9] concluded analytically that the rise in temperature and pore pressure were, respectively, 200 K and 0.2–2 MPa during the movement of the San Andreas Fault zone with an average stress of 10 MPa.

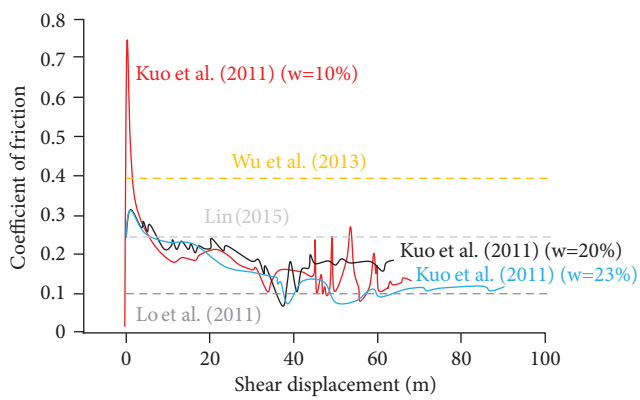

Figure 1: Different friction model for the initiation of the Hsien-du-shan landslide.

Miller et al. [10] calculated the excess pore pressure of a fault using the porosity reduction mechanism. Iverson [8] proposed that landslide motion is regulated by α, which depends on the dilatancy angle and the intrinsic timescales for pore pressure generation and dissipation. When $\alpha < 0$, soil in the shear zone contracts during slope failure. Then, the shear zone causes positive pore pressure feedback and runaway acceleration. Conversely, when $\alpha > 0$, slow and steady landslide motion occurs while positive pore pressure is supplied by rain infiltration.

Currently, knowledge of the shear behavior of rock avalanches is rather limited, especially when sliding occurs at a great depth. Fortunately, the ring shear apparatus has two obvious advantages for investigating the initiation of a rock avalanche: (1) there is no change in the cross-sectional area of the shear plane as the test proceeds; and (2) the sample can be sheared through an uninterrupted displacement of any magnitude [11].

Table 1 shows the available ring shear tests. Developing a CU ring shear test apparatus is crucial to clarify the coupling of landslide motion and pore pressure feedback. In addition, ring shear tests have focused on sand [12, 13] and clayey soils [14–18]. Moore and Iverson [18] concluded that although dilation reduces the internal friction angle of dry granular materials, pore expansion in fluid-saturated materials increases friction and strength by reducing pore-fluid pressure and increasing normal stresses at grain contacts. Atterberg limits, particle shapes, and shearing rates strongly govern stress fluctuations [17], although the particle size distribution is an additional factor for controlling the residual shear strength [19] in ring shear tests.

The maximum depth of the Hsien-du-shan rock avalanche was 85.6 m [20] based on the topographic data before and after the sliding event. In this study, the unit weight of the soils is assumed to be $\gamma = 27.1$ kN/m^3. The maximum normal stress may exceed 2000 kPa. In Table 1, although the designed maximum normal stresses of the DPRI-4, DPRI-5, and DPRI-6 exceeded 2000 kPa, a successful case study indicating a maximum normal stress exceeding 2000 kPa was lacking. Although the DPRI-7 achieved a successful maximum normal stress of up to 750 kPa, Sassa et al. [21] raised the issue regarding the poor performance of a servo-control system. Therefore, only the ring shear test devices proposed by Liao et al. [22], ICL-2 [23], and Wu et al. [24] would fulfill the desired high normal stresses that occurred at the Hsien-du-shan rock avalanche. This study presents an improvement in the ring shear device proposed by Liao et al. [22] and Wu et al. [24] to monitor the pore water pressure and the shear behavior of the soil/rock interface of the Hsien-du-shan rock avalanche.

2. The New Ring Shear Apparatus

The ring shear box consists of the upper ring shear box (Figure 2(a)) and the lower shear box (Figure 2(b)). For the ring shear apparatus only for the soils ([15, 25]; https://www.youtube.com/watch?v=R9vTsrE8bSA), the rough interface or vanes must be installed at the top and the bottom shear boxes to ensure that the shear failure occurs in the soils but not the interface of the shear box and the soils. In this study, the apparatus was designed to investigate the interface of two rock samples or of the rock and the soil. Rock sample is adhered to the upper shear box, and the interface between the rock sample and the top shear box is flat (Figure 2(a)). The soils are installed to the lower ring shear box (Figure 2(c)).

This ring shear system consists of an MTS, ring shear box, ring displacement control system, signal generator, and data acquisition system (Figure 3(a)). The MTS applies the normal stresses and measures the normal displacement and torque in the ring shear tests. The axial force and torque capacities of the MTS are 50 kN and 500 N-m, respectively. The ring shear box (Figure 3(b)) comprises the upper and lower boxes and is capable of functioning a maximum normal loading of 100 kN. When investigating the interface of the two rock samples, an epoxy is used to adhere rock specimens to both the upper and lower shear boxes [26]. However, when a soil-rock interface is investigated, the rock sample is adhered to the upper shear box, and the soils are put in the lower shear box. The ring displacement control system below the lower shear box, with a large displacement and rotational speeds ranging from 0.0018–1.8 mm/min, drives the lower shear box during the shearing tests. In each testing, the Square Teflon O-rings are, respectively, attached on the inner and outer sides of the samples, in the upper and lower shear boxes, to prevent extrusions water and soils.

In this study, the inner and outer diameters of the ring-shaped specimen are 11.0 cm and 14.9 cm, respectively. The inner and outer radius ratio is $n = 0.74$. The designs meet the dimensional requirements for a specimen as suggested by (1) [11] and (2) [27], for obtaining a uniform distribution of stress on the shear plane.

$$n = \frac{R_i}{R_o} = \frac{D_i}{D_o} \geq 0.71, \quad (1)$$

$$n = \frac{R_i}{R_o} = \frac{D_i}{D_o} \geq 0.65, \quad (2)$$

where R_o is the specimen outer radius, R_i is the specimen inner radius, D_o is the specimen outer diameter, D_i is the

Table 1: The sample size of ring shear test (modified by [39]).

Author	Inner diameter, D_i (cm)	Outer diameter, D_o (cm)	n (D_i/D_o)	Sample	Max. normal stress (kPa)	Pore pressure monitoring
Bishop et al.	10.16	15.24	0.67	Clay	980	N
Hungr and Morgenstern	22.00	30.00	0.73	Coarse sand, sand-rock flour mixtures, and polystyrene beads	200	N
Tika and Hutchinson [40]	10.16	15.24	0.67	Cohesive soil	980	N
Garga and Sendano	9.20	13.30	0.69	Sand	660	N
Sassa (DPRI-3)	21.0	31.0	0.68	Soils	500	Y
Sassa (DPRI-4)	21.0	29.0	0.72	Coarse grain sandy soil	3000	Y
Sassa (DPRI-5)	12.0	18.0	0.67	Soils	2000	Y
Sassa (DPRI-6)	25.0	35.0	0.71	Sands	3000 (designed) 750 (success)*	Y
Sassa (DPRI-7)	27.0	35.0	0.77	Silica sand	500	Y
Iverson et al. [16]	48.5	60.0	0.81	Tills	400	N
Liao et al. [22]	11.0	14.9	0.74	Sandstone	12,600 (designed) 4000 (success)**	N
Ostric et al. [41] (ICL-1)	10.0	14.0	0.71	Marl	1000	Y
Tomasetta et al. [42]	6.0	12.0	0.50	Fine powders	14.795	N
Hoyos et al. [15]	9.65	15.24	0.63	Soils	732	Y (suction)
Sassa et al. [23] (ICL-2)	10.0	14.2	0.70	Sands	3000	Y
Jeong et al. (2014)	11.0	25.0	0.44	Gravelly sandy soil	100	Y
Wu et al. [24]	11.0	14.9	0.74	Sandstone/remolded shale	4000	N
This study	11.0	14.9	0.74	Sandstone/remolded shear gouge	2710	Y

*Normal stress servo-control system does not function well. Tests were conducted to 750 kPa by changing the normal stress load cell [21]; **successful case study of the Tsaoling landslide during the Chi-Chi earthquake [22].

specimen inner diameter, and n is the ratio of the inner radius to the outer radius.

The normal and shear stresses applied to the shear zone of the specimen are represented by (3), (4), and (5):

$$\sigma_n = \frac{F_n}{\pi\left(R_o^2 - R_i^2\right)}, \tag{3}$$

$$M = 2\pi\int_{R_i}^{R_o} \tau \cdot r^2 dr = \frac{2\pi\tau\left(R_o^3 - R_i^3\right)}{3}, \tag{4}$$

$$\tau = \frac{3M}{2\pi\left(R_o^3 - R_i^3\right)}, \tag{5}$$

where σ_n is normal stress, τ is shear stress, F_n is normal force, M is torque, and R_i and R_o are the inner and outer radii, respectively.

When the ring shear tests start, a stress-controlled normal stress is applied from the upper shear box to consolidate the soil samples, and then the ring displacement control system below the lower shear box drives the lower shear box at a specified shear rate. The shear resistance along the shear plane, the interface of the samples, is measured.

During the ring shear test, the sliding surface must ensure a high water tightness, and the pore pressure cell installation must be adjoining to the sliding surface to accurately measure the changes in sliding-induced pore pressures. In the new ring shear apparatus, a drainage pipeline is drilled in the lower shear box slightly lower than the Teflon square O-ring and is adjoined to the sliding surface (Figure 3(b)). Note that if the pressure cell is directly attached to the drainage pipeline, the rotating ring shear test apparatus under a large shear displacement may tie up the pore pressure cell cable and break the pore pressure cell. To avoid the pressure cell damage, the drainage pipeline is connected to a pore pressure cell by a flexible tube to monitor the pore pressure of the shear plane (Figure 3(c)). The flexible tube is connected to the drainage pipeline after setting rock samples to the ring shear test apparatus, and the infilling water to the hollow acrylic cover should fill up the tube and the pipeline (Figure 3(b)). The pore pressure cell should be connected to the flexible tube below the water table and then is attached to the top of the acrylic cover (Figure 3(c)) before the shear test starts. The water tightness of the new ring shear apparatus was assured by Wu [28], in which the pore pressure reduced from its initial state of 125 to 120 kPa within 20 hours. The dilatancy or contraction at the shear plane during shearing can be obtained from changes in the specimen height.

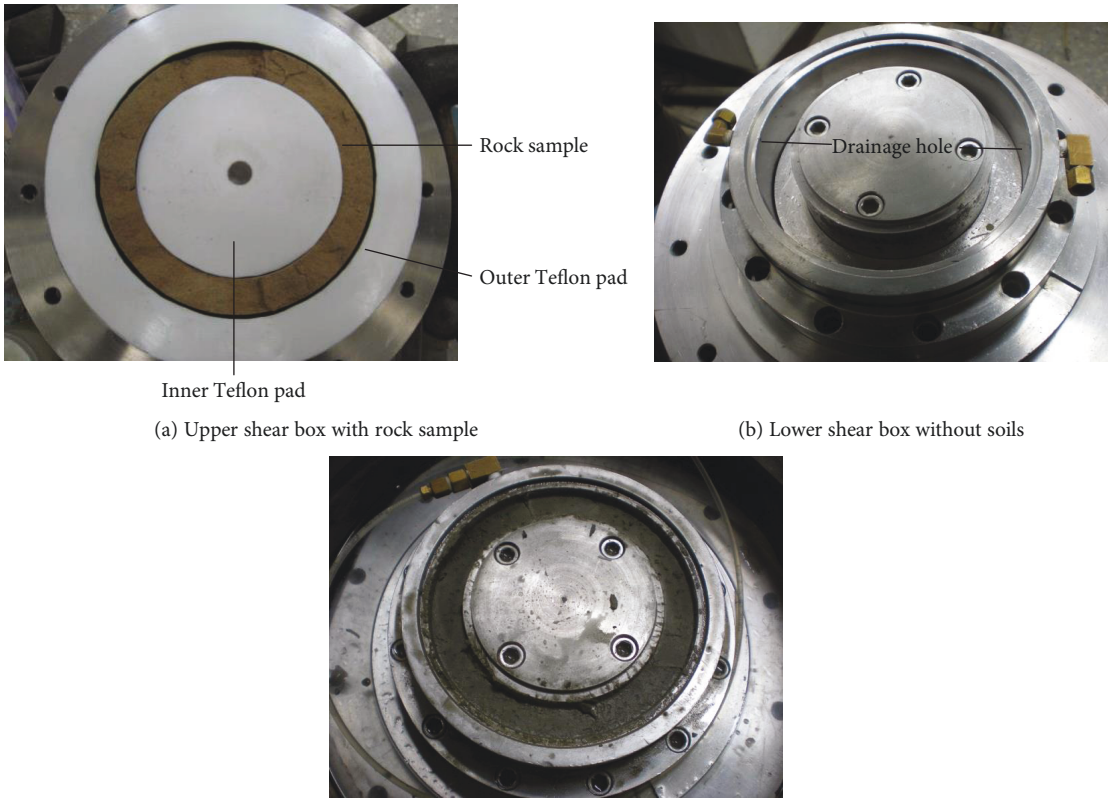

(a) Upper shear box with rock sample

(b) Lower shear box without soils

(c) Lower shear box with soils

Figure 2: Ring shear box.

3. The Hsien-du-shan Rock Avalanche

Figure 4 shows the rainfall data during Typhoon Morakot in 2009 recorded at the Chiahsien Station, which is the nearest rainfall station to the Hsien-du-shan landslide site in Kaohsiung County, Taiwan. The cumulative rainfall exceeded 2000 mm. The Hsien-du-shan rock avalanche occurred at 6:09 a.m. on August 9 and resulted in compound disasters, comprised of slope failure, landslide dam, and dam breakage, claiming more than 400 local residents of Hsiaolin village near the toe of the slope in Kaohsiung (Figure 5).

The shear strength parameters of the sliding surface are key factors when investigating a failure mechanism. Studies by Kuo et al. [7] indicated that the static friction as the peak coefficient of friction is between 0.3 ($ø = 16.7°$) and 0.75 ($ø = 36.9°$), with a normal stress = 1.0 MPa, when the water content of local colluvium is between 9 and 25% (Figure 1). When the rotary shear speed reaches 1.3 m/s, significant slip weakening occurs, and the coefficient of friction drops to a range between 0.1 ($ø = 5.71°$) and 0.2 ($ø = 11.3°$). The experimental results of the rotary shear test clarify that the shear strength of the sliding surface decreases remarkably when the landslide accelerates. Wu et al. [2] applied conventional direct shear tests to the high water content remolded soil obtained from the sliding slope of the Hsien-du-shan slope and suggested the normal stresses of 0.5, 1.0, 2, and 3.49 MPa for the experimental testing. The shear strength parameters of the high water content remolded soil are $c =$ 0 kPa and $ø = 21.4°$. In addition, Lin et al. [29] concluded that the shear strength parameters of the interface between the Tangenshan sandstone and the remolded Yenshuikeng shale, exhibiting high water contents, were $c = 0.0$ and $ø = 24.3°$ as determined by conventional direct shear tests. Then, the studies validated the stability of the Hsien-du-shan slope under the impact of the Chi-Chi earthquake in 1999 and the Heng-Chun earthquake in 2006. In fact, due to the absence of well-installed in situ groundwater monitoring instruments, the pore pressure change of the Hsien-du-shan sliding surface during its initiation is difficult to be obtained. In addition to field monitoring, Kuo et al. [7] and Wu et al. [2] have also difficulties in monitoring the pore pressure changes in experimental shear tests.

3.1. Geological Outline. The Hsien-du-shan slope is located at the east wing of the Hsiaolin syncline. The Hsiaolin syncline axis is located at the toe of the slope near the Hsiaolin Village and is east of the Chishan River [30–32]. A shear zone was discovered at the south boundary of the Hsien-du-shan rock avalanche [32].

The topographic and elevation differences in the source area before and after the occurrence of a landslide can be used to obtain the volume and maximum thickness of the sliding mass, respectively. The obtained values are carefully considered for maximum normal stress during the shear tests. Chen and Wu [20] calculated that the slid volume of the Hsien-du-shan rock avalanche was c.a. $27.118 \times 10^6\ m^3$

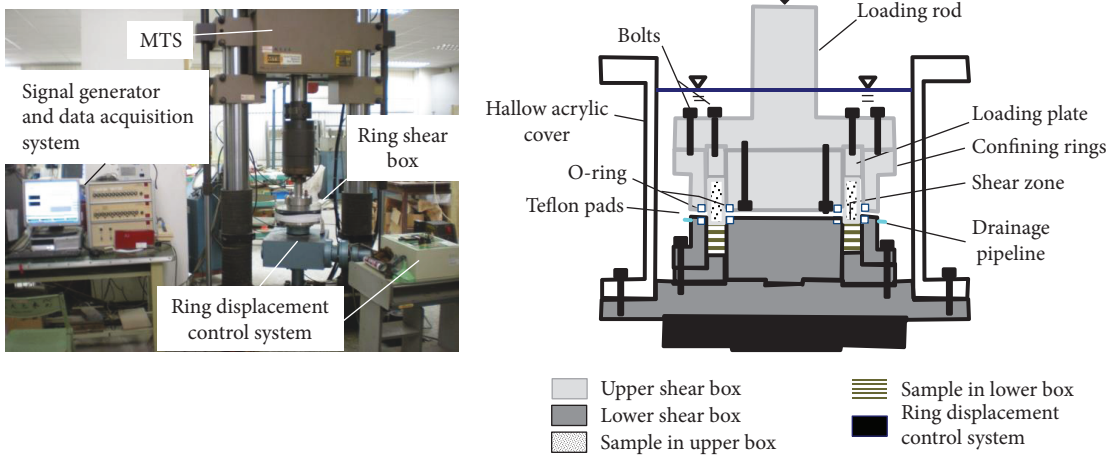

(a) Ring shear test system

(b) Sketch of the ring shear box

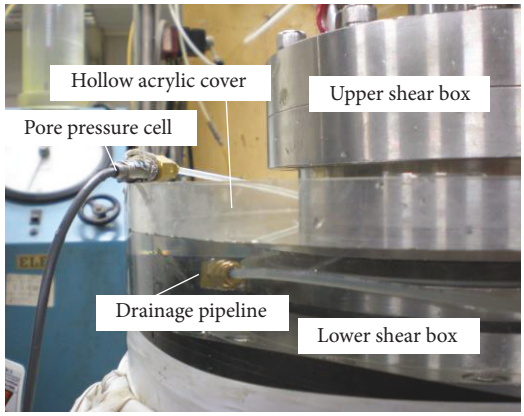

(c) Arrangement of the pore pressure cell

Figure 3: New pore pressure monitoring ring shear test apparatus.

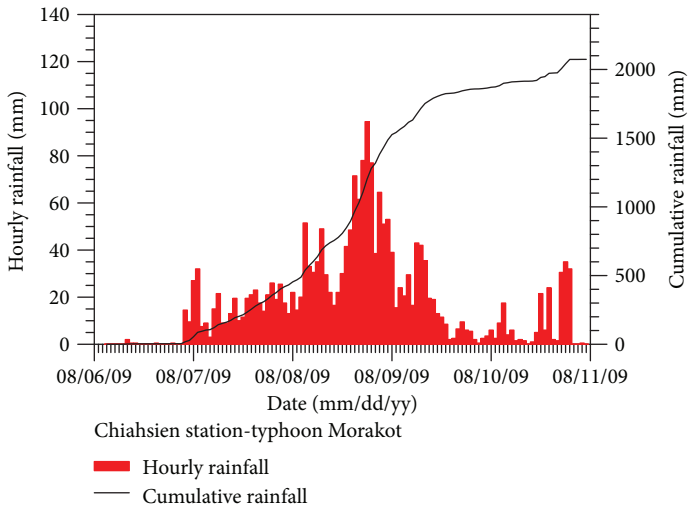

Figure 4: Rainfall data at the Chiahsien station.

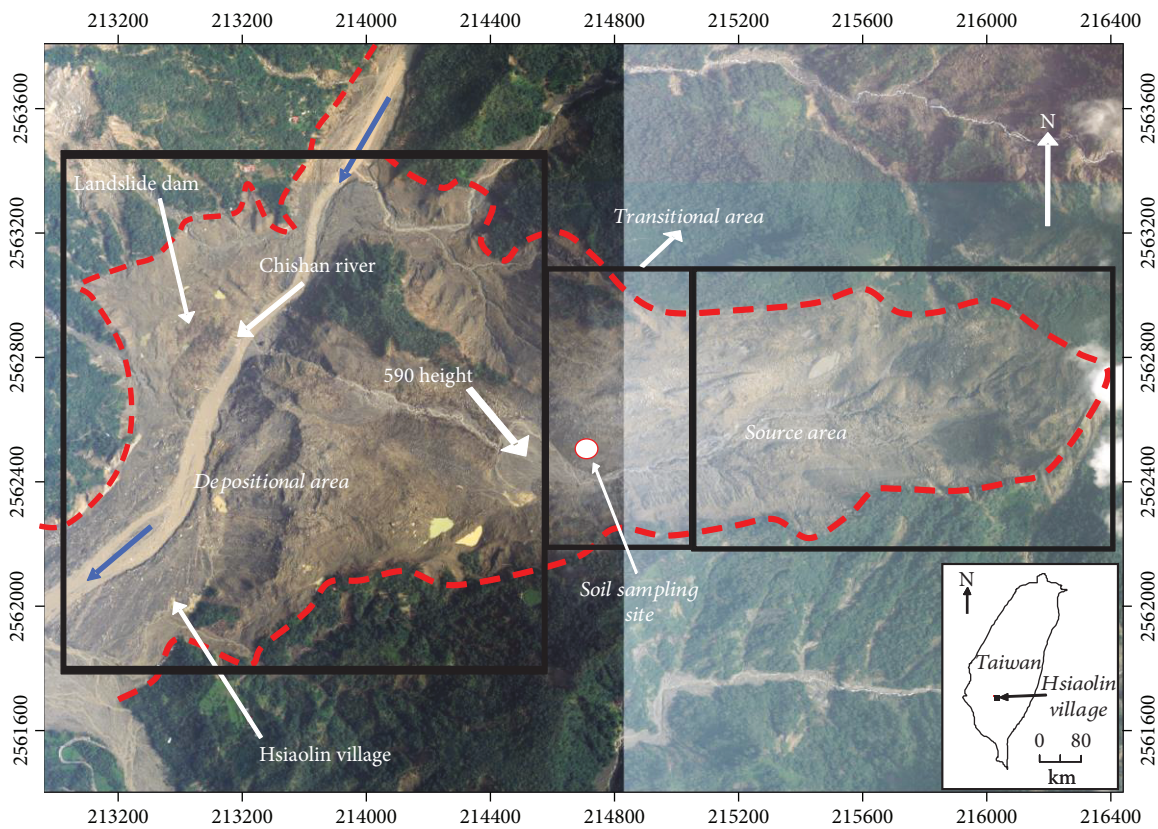

Figure 5: Aerial photo of the Hsien-du-shan rock avalanche.

and the maximum sliding thickness was 85.6 m using a 5 m × 5 m Digital Elevation Model before and after the landslide. The sliding surface is located at the interface of the fractured and weathered Yenshuikeng shale at the top and the Tangenshan sandstone at the bottom [30]. The water content of the sliding surface was high because the rock avalanche was triggered by heavy rainfall. Gravitational slope deformations were observed as unstable precursors before slope failure [2, 32].

4. The Consolidated Undrained Ring Shear Tests

4.1. Sample Preparation. In 2009 and 2010, the sliding gouges still covered the Tangenshan sandstone formation near the source area post the landslide event. The yellow sliding gouge implies that the gouge was generated as a filling layer at the interface of the Yenshuiken shale and Tangenshan sandstone prior to the incident of the landslide. In addition, the results of the X-ray diffraction analysis indicated that the minerals in the sliding gouge are very close to those observed in the Yenshuikeng shale [33]. To better understand the shear behavior of the sliding surface of the Hsien-du-shan rock avalanche, the interface between the sliding gouge and the Tangenshan sandstone is also investigated.

4.1.1. The Tangenshan Sandstone Sample. Tangenshan sandstones were obtained at the slope near the east edge of the 590 height (Figure 5), whose elevation is 590 m above the sea level. The physical and mechanical properties of the obtained Tangenshan sandstone are shown in Table 2. The uniaxial compressive strength and Young's modulus of the sandstone decrease significantly as the water content increases. In addition, the slake-durability index of the sandstone is $Id_1 = 99.03–99.29$ and $Id_2 = 98.39–98.76$. Based on the Gamble classification, sandstone is classified as a very high-durability rock [34].

Hollow cylinder samples with an inner diameter of 11.0 cm and an outer diameter of 14.9 cm are drilled from the retrieved rocks. The cylinders are cut with a height of 5 ± 0.2 cm to satisfy the size requirements of the ring shear box (Figure 6).

4.1.2. The Remolded Landslide Gouge. Due to the precipitous landform, a sufficient number of the gouges at the sliding surface of the source area were unavailable. In this study, the sandstones and the gouge at the sliding surface were taken in the transitional zone (Figures 5 and 7(a)). Therefore, the gouges are remolded to investigate the postpeak shear behavior because of the unstable topographical precursors before the landslide [2, 32]. In addition, Japanese landslide case studies [35] showed good agreement between the residual friction angles determined from undisturbed samples and remolded specimens using ring shear tests.

In Figure 7(a), only the gouges at the depth adjoining to the underlying Tangenshan sandstone were taken to avoid mixing external debris at the ground surface during slope failure (Figure 7(b)). Table 3 shows the physical properties

Table 2: Physical and mechanical properties of the Tangenshan sandstone.

Properties	Value
Air-dried unit weight, γ_d (kN/m^3)	24.40–25.25
P-wave velocity, V_p (m/s)	2463.24–2692.51
S-wave velocity, V_s (m/s)	1477.94–1549.23
Uniaxial compressive strength, σ_c (MPa)	
Air-dried sample with water content = 0.72%	64.96–73.52
High water content sample with water content = 2.85%	48.44–61.80
Young's modulus, E (MPa)	
Air-dried sample with water content = 0.72%	7885.98–9488.41
High water content sample with water content = 2.85%	3014.21–4962.34
Slake-durability index (%)	
Id_1	99.03–99.29
Id_2	98.39–98.76

Figure 6: Hollow cylinder sample of the Tangenshan sandstone.

of the landslide gouge, which are classified to be CL based on the Unified Soil Classification.

The procedures for preparing the remolded local soils for the consolidated undrained (CU) ring shear tests include the following:

Step 1. Soils are passed through a no. 10 sieve to reduce the impacts of large grains on the shear test because the thickness of the sample is 2 cm. The lower shear box is installed in the ring displacement control system (Figure 3). Then, the lower shear box is filled with the dry gouges until the groove for the square Teflon O-ring.

Step 2. At the Hsien-du-shan slope, the landslide gouge is located above the Tangenshan sandstone. However, in the ring shear test, the arrangement of the Tangenshan sandstone sample above the remolded gouges (Figure 8) is opposite to the in situ case on the Hsien-du-shan slope. The upper and the lower shear boxes are integrated into the ring shear apparatus. The specified normal force is applied to the soil sample in dry conditions for 12 hours. Then, the interface of the remolded landslide gouge and sandstone sample is submerged in water for an additional 36 hours for the CU ring shear tests considering that the Hsien-du-shan landslide was triggered by heavy rainfall.

4.2. Identification of Test Parameters. The area of the ring shear sample, A, is 79.33×10^{-4} m^2 because the outer and inner diameters of the sample are 14.9 and 11.0 cm, respectively. The normal forces used in the tests are calculated by the equation $F_n = \gamma \times \text{Dep} \times A$. In the CU tests, the normal force, F_n, to consolidate the remolded landslide gouge is 21.5 kN, considering the maximum depth of the Hsien-du-shan rock avalanche was roughly 100 m based on the topographic data before and after the landslide. Then, three normal forces, N_{50} = 10.75 kN, N_{75} = 16.125 kN, and N_{100} = 21.5 kN, corresponding to depths (Dep) of 50 m, 75 m, and 100 m, respectively, covered the normal force calculated from the maximum sliding thickness of 85.6 m [20] and are applied in the ring shear tests.

Vertical displacement of the sample in each test is monitored using the LVDT of the MTS from the beginning of the consolidation. A pore pressure sensor having a full capacity of 500 kPa, manufactured by Kyowa, Japan, is connected to the drainage pipeline beneath the water table at the lower ring shear box (Figure 3(b)) before the ring shear test starts. The ring displacement control system below the lower shear box (Figure 3(a)) controls the shear rate of 1.5 mm/min (1.3 degree/min) for the CU shear test after the normal stress, converging the vertical displacement, is applied. The normal and shear stresses are computed by incorporating the measured axial force and torque to (3) and (5). Subsequently, the curves of the shear stress-shear displacement, normal displacement-shear displacement, and pore water pressure change-shear displacement are plotted.

5. Experimental Results

CU ring shear tests were conducted on the interface of the Tangenshan sandstone and the remolded landslide gouges to clarify the mechanical behavior of this surface under large shear displacement. Figure 9 shows the CU ring shear test results under the three normal forces, N_{50} = 10.75 kN, N_{75} = 16.125 kN, and N_{100} = 21.5 kN. For each ring shear test, the sample was sheared for 3 cycles (rotation angle = 1080°; shear displacement = 1218 mm). The experimental time is approximately 13.5 hours under the shear rate of 1.5 mm/min.

The Mohr-Coulomb failure criterion (Figure 10) is obeyed to interpret the corresponding shear stresses by the three designed normal stresses, N_{50}, N_{75}, and N_{100}, based on the shear stress-shear displacement curves (Figure 9). Figure 10 shows the minimum, average, and maximum residual strengths of the ring shear tests in each shear circle. The total stress failure criteria of each shear circle show that the cohesion of the sliding interface is 0.0 kPa. In addition, the internal friction angles are $\varnothing = 25.3°$ (coefficient of friction = 0.480), 26.1° (coefficient of friction = 0.491), and 25.3° (coefficient of friction = 0.473) for shear circles 1, 2, and 3, respectively. The total stress failure criteria changed insignificantly when the shear distance is within 1218 mm, which can be considered as a landslide initiation (Figure 10).

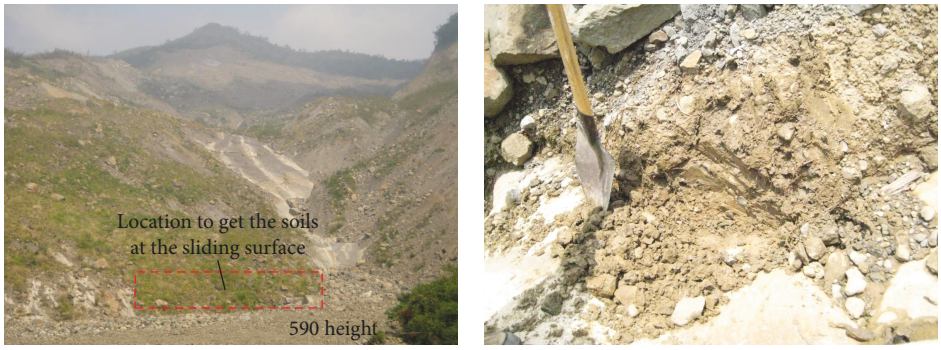

(a) Location to get the soils at the sliding surface (b) Picture to get the landslide gouge

Figure 7: Soil sampling at the sliding slope.

Table 3: Physical properties of local landslide gouge.

Sample number	Sample 1	Sample 2	Sample 3
Specific gravity (G_s)	2.711	2.709	2.696
Liquid limit (LL)	29.39	28.84	29.51
Plastic limit (PL)	14.42	15.90	15.22
Plastic index (PI)	14.97	12.94	14.29
D_{10} (mm)	0.01247	0.00909	0.01097
D_{30} (mm)	0.06612	0.06545	0.05478
D_{60} (mm)	0.07304	0.07254	0.07099
Uniform coefficient, C_u	5.857	7.977	6.469
Coefficient of gradation, C_c	4.798	6.494	3.852
Unified soil classifications	CL	CL	CL

Comparing this experimental data to the available shear strength parameters of the Hsien-du-shan sliding surface (Figure 1), the ring shear test results are close to the data obtained from conventional direct shear tests, $\varnothing = 21.4^\circ$ [2]. However, this new ring shear test provides higher strengths than the strengths determined by high-speed rotary shear tests with a water content exceeding 20% [7] (coefficient of friction = 0.1 to 0.2), numerical simulations [6] (coefficient of friction = 0.1), or the topographic map [1, 2] (coefficient of friction = 0.23). Studies by Kuo et al. [7] and Lo et al. [6] focused on investigating slip weakening of the sliding surface under high speed and very large shear movements. Rock mass disintegrations and the high sliding speed are key factors in decreasing the friction angle [2, 7] of the postfailure rock mass. However, the objective of this study is to investigate the slope failure initiation. The internal friction angles of the sliding surface investigated by the ring shear test, $\varnothing = 25.3^\circ$ to 26.1°, are larger than the dip angle of the slope (Figure 5), which clarifies that the Hsien-du-shan slope was stable before Typhoon Morakot.

In addition, in Figure 9, the sliding interface undergoes shear contractions when normal stresses corresponding to depths of 50, 75, and 100 m are applied. The slope of the axial stroke vs. shear displacement curve is defined as $\tan\psi$. The dilatancy angle, ψ, is positive in the case of dilative shearing, but this value is negative in the case of contractive shearing. The value of ψ evolves as shear displacement proceeds, and $\psi \to 0$ indicates that these shear displacements are large enough that the deforming soil in the shear zone approaches a constant critical state porosity.

The flexible tube connecting the drainage pipeline and the pore pressure cell (Figure 3(b)) is full of water and is returned to zero before the ring shear test starts. Figure 9 shows the pore pressure variation during the shear test. Shear contraction increases pore pressure during the ring shear tests. However, pore pressures decrease in the first 2 shear cycles in all the ring shear tests. The pore pressure decrease during the initial stage of the ring shear tests may be due to the unsaturated remolded landslide gouge even if it is put in water and is consolidated for 36 hours. When the sample is fully saturated, the shear contraction (Figure 9) increases the pore pressures in an undrained condition. Oppositely, water may flow into the shear face and decrease the pore pressure.

Table 4 shows the water contents of the remolded landslide gouge cross section and rock samples after the ring shear tests. The water contents of the remolded landslide gouge are between 8.82 and 14.49%, varying within 2% in the cross section. The water content is close to the PL of the landslide gouge (Table 3) and is within the range for in situ colluvium, which is between 9 and 25% [7]. The increase in pore pressures caused by the shear contraction implies that the effective normal stress and slope stability both decrease as the shear displacement increases after the onset of the sliding. In addition, an increase in the consolidating pressure increases the density but decreases the hydraulic conductivity of the remolded landslide gouge. Therefore, by considering both the long shear displacement of the rock avalanche and the large normal stress, the pore pressure would increase significantly and continuously (Figure 9).

The new CU ring shear tests provide additional remarks to clarify the initial sliding behavior of the Hsien-du-shan rock avalanche:

(1) The sliding surface is in the postpeak state because of unstable topographical precursors before the landslide [2, 32]

(2) After the landslide starts, the CU ring shear test results indicate that shear contractions would occur

(a) Sample in the ring shear apparatus

(b) Integrated samples

Figure 8: Sample arrangement for the ring shear test.

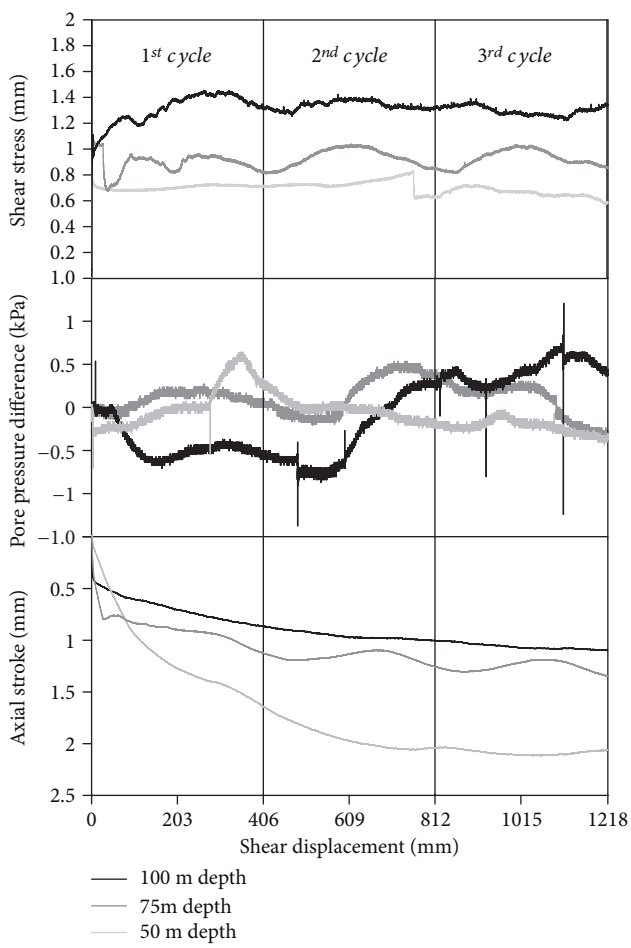

Figure 9: Experimental results of CU ring shear test.

at the sliding surface leading to a large increase in the pore pressure. Iverson [8] has also supported that the increasing pore pressure would further accelerate the sliding. In addition, a deep sliding surface with a high normal stress results in a landslide gouge with low hydraulic conductivity, which dissipates the pore pressure later

(3) The ring shear test results with a shearing rate of 1.5 mm/min are close to the data from conventional direct shear tests, $\varnothing = 21.4^\circ$ [2]. Both shear tests got the shear strength parameters when the landslide was initiated with slow shearing rate but not the whole sliding process. The sliding velocity of the Hsien-du-shan landslide is estimated from 20.4 to 33.7 m/s [32]. Yang et al. [36] indicated that the shear rate controls the shear behavior of a sliding surface. When the sliding surface is accelerated to a high speed, the slip weakening [7] governs the mechanical properties of the sliding surface. In addition, Wu [37] showed that the disintegration of the rock mass during a landslide increases the run-out distance of the sediments. Therefore, the slip weakening at the sliding surface and the disintegration of the blocky rock mass are the two main reasons that the internal friction angle of the sliding surface determined by the ring shear test ($\varnothing = 25.3^\circ$ to 26.1°) surpassed the apparent friction angle ($\varnothing = 13^\circ$), which is defined as the ratio of the vertical height and the horizontal travel distance of a landslide, suggested by the topography [2]. Further verifications can be carried out by a discrete element method with the slip weakening algorithm [38] in the future

6. Conclusions

In this study, a new ring shear apparatus capable of conducting a CU shear test was developed. The capacity of the new device is ascertained by the successful modelling of the initiation of the heavy rainfall-induced Hsien-du-shan rock avalanche at the sandstone/landslide gouge interface with a maximum normal stress exceeding 2 MPa. Furthermore, the shear behaviors of the sliding surface under the different normal stresses were explored.

The experimental results indicated that the remolded landslide gouge governs the shear behavior of a high water content sliding surface such as the Hsien-du-shan rock avalanche. The internal friction angle of the sliding surface in the total stress state investigated by the ring shear test falls between 25.3 and 26.1°, which is larger than the dip angle

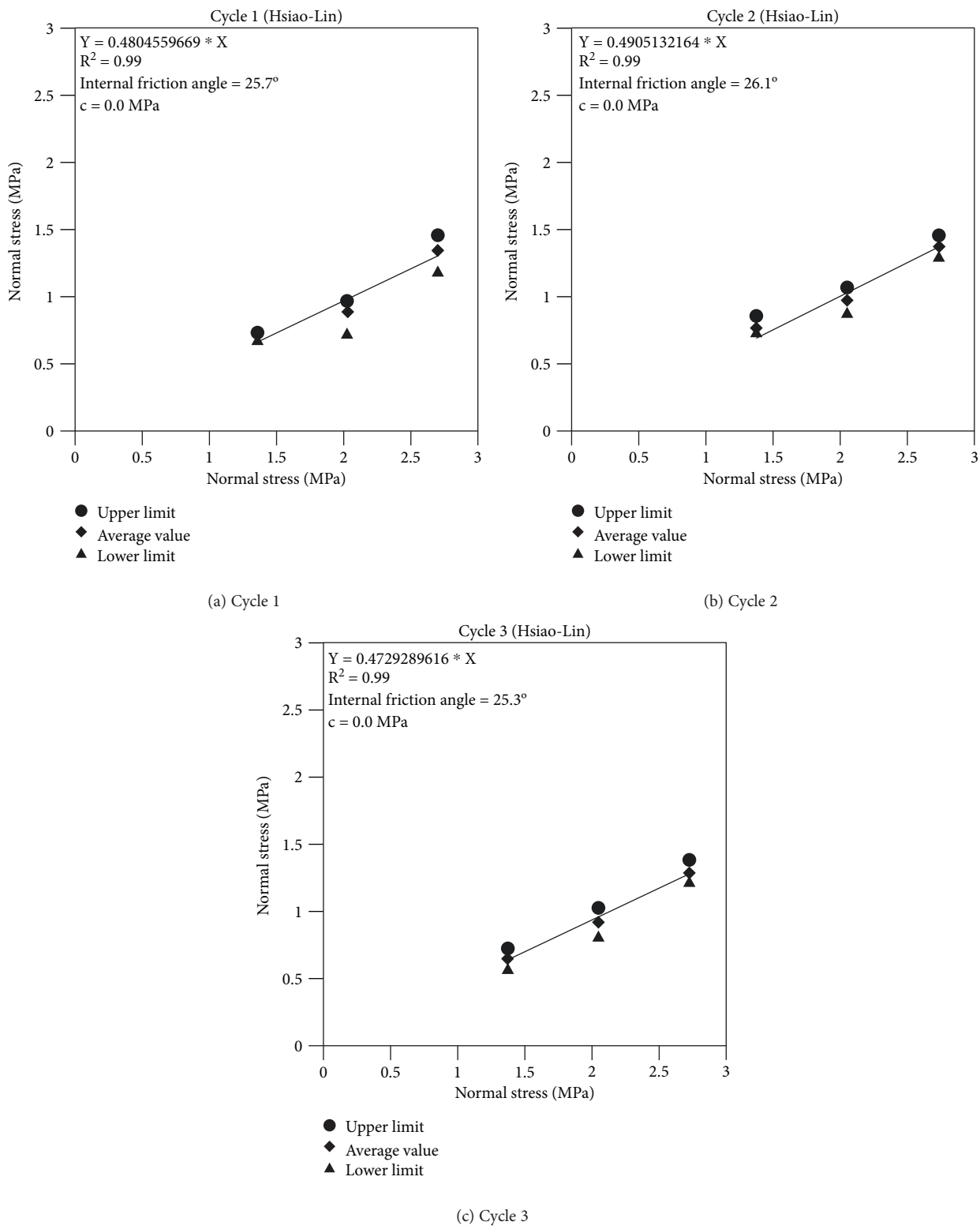

Figure 10: Failure criteria of the sliding interface.

of the slope and thus clarifies the stability of the slope before Typhoon Morakot.

When the movement of the sliding interface initiated, the shear contraction at the sliding surface generates excessive pore pressure feedback and destabilizes the slope. In addition, the low hydraulic conductivity of the landslide gouge/sandstone interface would result in the significant and continuous pore pressure increase during the long shear

Table 4: Water content of the samples after ring shear test.

Sample		Depth = 100 m	Depth = 75 m	Depth = 50 m
	Upper part	8.82%	14.49%	10.56%
Remolded landslide gouge	Middle part	10.03%	11.83%	10.29%
	Lower part	9.93%	12.00%	9.88%
Tangenshan rock		1.94%	2.13%	—

displacement when the sliding surface is sheared under large normal stresses. The excessive pore pressure can accelerate the rock avalanche.

Data Availability

The data used to support the findings of this study are available from the corresponding author upon request.

Conflicts of Interest

The authors declare that they have no conflicts of interest.

Acknowledgments

The authors appreciate their colleagues in the rock laboratory of the Department of Civil Engineering, National Cheng Kung University, Taiwan, for their kind help during rock gathering and sample preparations. In addition, thanks are due to the National Science Council of Taiwan (NSC 92-2211-E-426-003) and the Ministry of Science and Technology of Taiwan (MOST 107-2625-M-006-014) for their financial support. Special thanks are due to the reviewers and Prof. Ching Hung for his valuable comments.

References

[1] W. K. Lin, *Simulating the Rock Avalanche by Three Dimensional Distinct Element Method, [M.S. Thesis]*, National Cheng Kung University, Tainan, Taiwan, 2015.

[2] J. H. Wu, J. H. Chen, and C. W. Lu, "Investigation of the Hsien-du-shan rock avalanche caused by typhoon Morakot in 2009 at Kaohsiung county, Taiwan," *International Journal of Rock Mechanics and Mining Sciences*, vol. 60, pp. 148–159, 2013.

[3] M. Chigira, C. Y. Tsou, Y. Matsushi, N. Hiraishi, and M. Matsuzawa, "Topographic precursors and geological structures of deep-seated catastrophic landslides caused by typhoon Talas," *Geomorphology*, vol. 201, pp. 479–493, 2013.

[4] W. H. Schulz, "Landslide susceptibility revealed by LIDAR imagery and historical records, Seattle, Washington," *Engineering Geology*, vol. 89, no. 1-2, pp. 67–87, 2007.

[5] J. H. Wu, W. K. Lin, and H. T. Hu, "Post-failure simulations of a large slope failure using 3DEC: the Hsien-du-shan slope," *Engineering Geology*, vol. 242, pp. 92–107, 2018.

[6] C. M. Lo, M. L. Lin, C. L. Tang, and J. C. Hu, "A kinematic model of the Hsiaolin landslide calibrated to the morphology of the landslide deposit," *Engineering Geology*, vol. 123, no. 1-2, pp. 22–39, 2011.

[7] C. Y. Kuo, Y. C. Tai, C. C. Chen et al., "The landslide stage of the Hsiaolin catastrophe: simulation and validation," *Journal of Geophysical Research*, vol. 116, no. F4, 2011.

[8] R. M. Iverson, "Regulation of landslide motion by dilatancy and pore pressure feedback," *Journal of Geophysical Research*, vol. 110, no. F2, 2005.

[9] T. C. Lee and P. T. Delaney, "Frictional heating and pore pressure rise due to a fault slip," *Geophysical Journal International*, vol. 88, no. 3, pp. 569–591, 1987.

[10] S. A. Miller, A. Nur, and D. L. Olgaard, "Earthquakes as a coupled shear stress-high pore pressure dynamical system," *Geophysical Research Letters*, vol. 23, no. 2, pp. 197–200, 1996.

[11] A. W. Bishop, G. E. Green, V. K. Garga, A. Andresen, and J. D. Brown, "A new ring shear apparatus and its application to the measurement of residual strength," *Geotechnique*, vol. 21, no. 4, pp. 273–328, 1971.

[12] A. C. Trandafir and K. Sassa, "Undrained cyclic shear response evaluation of sand based on undrained monotonic ring shear tests," *Soil Dynamics and Earthquake Engineering*, vol. 24, no. 11, pp. 781–787, 2004.

[13] G. Wang and K. Sassa, "Seismic loading impacts on excess pore-water pressure maintain landslide triggered flowslides," *Earth Surface Processes and Landforms*, vol. 34, no. 2, pp. 232–241, 2009.

[14] J. A. Clausen, R. H. Gabrielsen, E. Johnsen, and J. A. Korstgård, "Fault architecture and clay smear distribution. Examples from field studies and drained ring-shear experiments," *Norwegian Journal of Geology*, vol. 83, no. 2, pp. 131–146, 2003.

[15] L. R. Hoyos, C. L. Velosa, and A. J. Puppala, "Residual shear strength of unsaturated soils via suction-controlled ring shear testing," *Engineering Geology*, vol. 172, pp. 1–11, 2014.

[16] N. R. Iverson, R. W. Baker, and T. S. Hooyer, "A ring-shear device for the study of till deformation: tests on tills with contrasting clay contents," *Quaternary Science Reviews*, vol. 16, no. 9, pp. 1057–1066, 1997.

[17] Y. R. Li and A. Aydin, "Shear zone structures and stress fluctuations in large ring shear tests," *Engineering Geology*, vol. 167, pp. 6–13, 2013.

[18] P. L. Moore and N. R. Iverson, "Slow episodic shear of granular materials regulated by dilatant strengthening," *Geology*, vol. 30, no. 9, pp. 843–846, 2002.

[19] Y. R. Li, B. P. Wen, A. Aydin, and N. P. Ju, "Ring shear tests on slip zone soils of three giant landslides in the Three Gorges Project area," *Engineering Geology*, vol. 154, pp. 106–115, 2013.

[20] S. C. Chen and C. H. Wu, "The geomorphological variation triggered by catastrophic deep landslide in Siaolin village," *Journal of Chinese Soil and Water Conservation*, vol. 40, pp. 359–376, 2009.

[21] K. Sassa, B. He, K. Dang, O. Nagai, and K. Takara, "Plenary: Progress in landslide dynamics," in *Landslide Science for a Safer Geoenvironment*, vol. 1, pp. 37–67, Springer, Cham, Switzerland, 2014.

[22] C. J. Liao, D. H. Lee, J. H. Wu, and C. Z. Lai, "A new ring-shear device for testing rocks under high normal stress and dynamic

conditions," *Engineering Geology*, vol. 122, no. 1-2, pp. 93–105, 2011.

[23] K. Sassa, K. Dang, B. He, K. Takara, K. Inoue, and O. Nagai, "A new high-stress undrained ring-shear apparatus and its application to the 1792 Unzen–Mayuyama megaslide in Japan," *Landslides*, vol. 11, no. 5, pp. 827–842, 2014.

[24] J. H. Wu, C. J. Liao, H. M. Lin, and T. T. Fang, "An experimental study to characterize the initiation of the seismic-induced Tsaoling rock avalanche," *Engineering Geology*, vol. 217, pp. 110–121, 2017.

[25] Y. Hong, G. Yu, Y. Wu, and X. Zheng, "Effect of cyclic loading on the residual strength of over-consolidated silty clay in a ring shear test," *Landslides*, vol. 8, no. 2, pp. 233–240, 2011.

[26] D. H. Lee, C. H. Juang, J. W. Chen, H. M. Lin, and W. H. Shieh, "Stress paths and mechanical behavior of a sandstone in hollow cylinder tests," *International Journal of Rock Mechanics and Mining Sciences*, vol. 36, no. 7, pp. 857–870, 1999.

[27] E. N. Bromhead, "A simple ring shear apparatus," *Ground Engineering*, vol. 12, no. 5, pp. 40–44, 1979.

[28] C. H. Wu, *Investigating the Residual Strength of the Soft Rocks at South Taiwan Using the Ring-Shear Test Apparatus, [M.S. Thesis]*, Department of Civil Engineering, National Cheng Kung University, Tainan, Taiwan, 2005.

[29] H. M. Lin, J. H. Wu, and E. Sunarya, "Stability analysis of Hsien-du-shan rock slope during the earthquakes," *Disaster Advances*, vol. 6, no. 10, pp. 4–10, 2013.

[30] C. T. Lee, J. J. Dong, and M. L. Lin, "Geological investigation on the catastrophic landslide in Siaolin village, southern Taiwan," *Sino-Geotechnics*, vol. 122, pp. 87–94, 2009.

[31] Q. C. Sung, C. W. Lin, W. H. Lin, and W. C. Lin, *Geologic Map and Explanatory Text of Taiwan Scale 1:50,000 51 Chiahsien*, CGS, MOEA, Taipei, Taiwan, 2000.

[32] C. Y. Tsou, Z. Y. Feng, and M. Chigira, "Catastrophic landslide induced by typhoon Morakot, Shiaolin, Taiwan," *Geomorphology*, vol. 127, no. 3-4, pp. 166–178, 2011.

[33] J. H. Wu, J. H. Chen, E. Sunarya, and T. N. Do, "Technical report of investigating and simulating the large landslides under global warming," National Science Council of Taiwan, Taipei, Taiwan, 2013.

[34] J. C. Gamble, *Durability–Plasticity Classification of Shales and other Argillaceous Rocks. [Ph.D. Thesis]*, University of Illinois Urbana Champaign, Urbana Champaign, Urbana, IL, USA, 1971.

[35] B. Tiwari, T. L. Brandon, H. Marui, and G. R. Tuladhar, "Comparison of residual shear strengths from back analysis and ring shear tests on undisturbed and remolded specimens," *Journal of Geotechnical and Geoenvironmental Engineering*, vol. 131, no. 9, pp. 1071–1079, 2005.

[36] C. M. Yang, W. L. Yu, J. J. Dong et al., "Initiation, movement, and run-out of the giant Tsaoling landslide — what can we learn from a simple rigid block model and a velocity–displacement dependent friction law?," *Engineering Geology*, vol. 182, pp. 158–181, 2014.

[37] J. H. Wu, "Applying discontinuous deformation analysis to assess the constrained area of the unstable Chiu-fen-erh-shan landslide slope," *International Journal for Numerical and Analytical Methods in Geomechanics*, vol. 31, no. 5, pp. 649–666, 2007.

[38] L. Z. Wang, H. Y. Jiang, Z. X. Yang, Y. C. Xu, and X. B. Zhu, "Development of discontinuous deformation analysis with displacement-dependent interface shear strength," *Computers and Geotechnics*, vol. 47, pp. 91–101, 2013.

[39] K. Sassa, H. Fukuoka, G. Wang, and N. Ishikawa, "Undrained dynamic-loading ring-shear apparatus and its application to landslide dynamics," *Landslides*, vol. 1, no. 1, pp. 7–19, 2004.

[40] T. E. Tika and J. N. Hutchinson, "Ring shear tests on soil from the Vaiont landslide slip surface," *Geotechnique*, vol. 49, no. 1, pp. 59–74, 1999.

[41] M. Ostric, K. Ljutic, M. Krkac et al., "Portable ring shear apparatus and its application on Croatian landslides," *Annuals of Disaster Prevention Research Institute, Kyoto University*, vol. 55, no. B, pp. 57–65, 2012.

[42] I. Tomasetta, D. Barletta, and M. Poletto, "The high temperature annular shear cell: a modified ring shear tester to measure the flow properties of powders at high temperature," *Advanced Powder Technology*, vol. 24, no. 3, pp. 609–617, 2013.